Journal of Electroanalytical Chemistry 856 (2020) 113601

Contents lists available at ScienceDirect

Journal of Electroanalytical Chemistry

journal homepage: www.elsevier.com/locate/jelechem

Polyol synthesized graphene/Pt_xNi_{100-x} nanoparticles alloy for improved electrocatalytic oxidation of methanol in acidic and basic media

Safaa A. Elsherif [a], Ehab N. El Sawy [b], Nabil A. Abdel Ghany [a,*]

[a] Physical Chemistry Department, National Research Centre, Dokki, 12622, Cairo, Egypt
[b] Department of Chemistry, School of Science and Engineering, American University in Cairo, New Cairo, 11835, Egypt

ARTICLE INFO

Keywords:
Polyol synthesis
Methanol oxidation
Graphene
Pt–Ni nanoparticles
pH effect

ABSTRACT

In this study, a series of graphene-supported Pt–Ni nanoparticles are successfully synthesized by a simple modified polyol method and used as electrocatalysts for methanol oxidation. In this method, graphene oxide is reduced to graphene and Pt–Ni alloy nanoparticles are deposited on graphene sheets simultaneously in ethylene glycol, which acts as a reducing agent. The electrocatalysts are physically characterized using X-ray diffraction (XRD), energy dispersive X-ray spectroscopy (EDS), thermal gravimetric analysis (TGA), high-resolution transmission electron microscopy (HRTEM), and scanning electron microscopy (SEM). The cyclic voltammetry and chronoamperometry electrochemical measurements in acidic and alkaline media are promising. The electrocatalysts containing Ni ($G/Pt_{75}–Ni_{25}$, $G/Pt_{54}–Ni_{46}$ and $G/Pt_{40}–Ni_{60}$) have higher catalytic activity and stability for the MOR than pure G/Pt in both acidic and alkaline media. $G/Pt_{54}–Ni_{46}$ has the highest performance in acidic and alkaline media, and its activity in alkaline media (2732 A/g_{Pt}) is nearly 10 times higher than that in acidic media (260 A/g_{Pt}). The superior catalytic performance in alkaline media may be because Ni is more stable in alkaline media. These electrocatalysts are promising candidates for direct methanol fuel cell (DMFC) anode catalysts.

1. Introduction

Future energy requirements necessitate a switch from fossil fuels to new energy sources that are environmentally friendly and renewable. A promising way to facilitate this switch is to use fuel cells to directly convert chemical energy into electricity. Among the different types of fuel cells, direct methanol fuel cells (DMFCs) have received much attention due to their numerous advantages, including high power density, high energy conversion, low operating temperature, and wide range of applications, such as use in automobiles, chargers, and laptops [1–3].

The major reactions in DMFCs are the methanol oxidation reaction (MOR) at the anode and the oxygen reduction reaction (ORR) at the cathode [4]. The poor kinetics of the MOR is a major barrier that restricts the commercial applications of DMFCs [5,6]. Pt is the best single-metal catalyst for electrocatalytic oxidation of methanol at an anode. However, its low tolerance to CO poisoning and high cost hinder its use for broad applications [7,8]. Using Pt-based bimetallic nanostructures, in which Pt is partially replaced by low-cost 3d transition metals, is a promising approach to solve this problem.

Alloying Pt with transition metals on the basis of bi-functional, electronic, and strain effects can decrease the amount of Pt and further increase its catalytic activity and poisoning tolerance under operating conditions [9,10]. Pt-based metallic catalysts (e.g., PtFe, PtNi, PtCu, PtAu, PtCo, and Pt–Fe–Co) that reduce Pt consumption have been studied for the ORR and MOR to minimize catalyst cost, enhance catalytic activity, and improve stability [11–16].

Among binary alloys, PtNi alloys are promising for the MOR because Ni is more cost-effective than other metals [17–19]. Additionally, as shown by X-ray photoelectron spectroscopy (XPS) results in previous studies, the incorporation of Ni can shift the Pt 4f peak to a lower binding energy, indicating electron transfer from Ni to Pt [20]. NiO_xH_y species in PtNi catalysts lower the oxidation potential of CO [21]. Thus, PtNi alloys can exhibit higher activity and better tolerance for the MOR than pure Pt.

The preparation method, pretreatment of materials and supporting materials are important factors that affect catalyst performance [22]. The supporting material has a major influence on the catalytic performance, stability, and consumption of the supported catalyst [23].

Several carbon materials have been examined as catalyst supports for DMFCs, such as vulcan carbon [24], carbon nanotubes (CNTs) [25,26], carbon nanofibres [27], and mesoporous carbon [28]. Vulcan carbon is a popular support; however, it has poor corrosion resistance under the working conditions in DMFCs [29]. Using pristine CNTs leads to poor

* Corresponding author.
E-mail addresses: na.abdelghany@nrc.sci.eg, na_manakhly@yahoo.co.uk (N.A. Abdel Ghany).

https://doi.org/10.1016/j.jelechem.2019.113601
Received 20 July 2019; Received in revised form 23 October 2019; Accepted 24 October 2019
Available online 18 November 2019

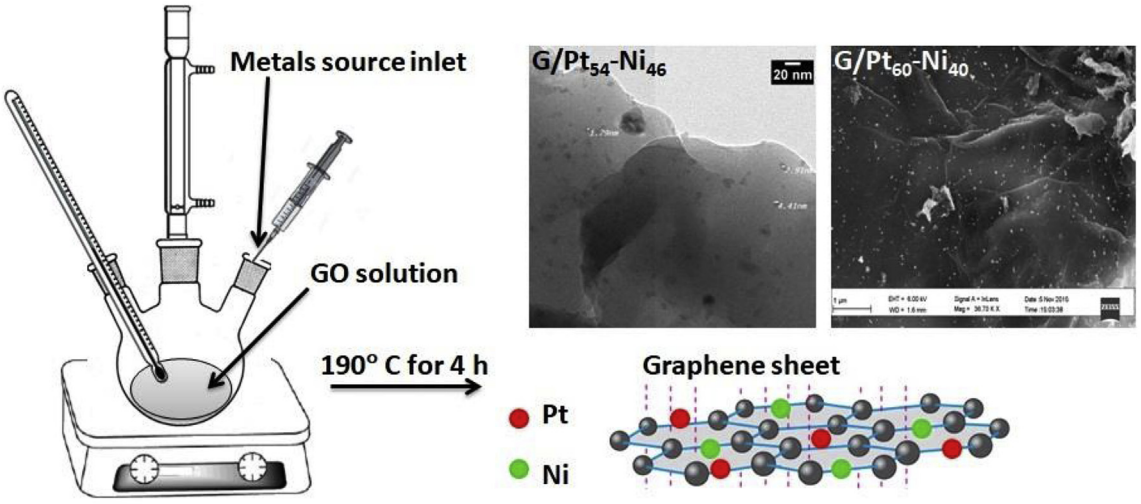

Scheme 1. Synthesis of Graphene/PtxNi100-x Nanoparticles.

stability and dispersal of the deposited catalyst [30]. Thus, finding a new carbon support material to achieve low Pt consumption, high catalytic activity, high stability, and good catalyst utilization is important.

Graphene, which is the core structure of all graphitic forms, has received attention because of its unique properties, including its high specific surface area, excellent conductivity, unusual electronic properties and ability to improve the catalytic properties of supported nanoparticles, resulting in an ideal catalyst support for DMFCs [31–33].

Many researchers have prepared graphene-supported nanoparticles (G/NPs) by adding graphene to a nanoparticles (NPs) synthesis mixture for in situ formation of NPs on G or by mixing NPs with G. However, these processes consist of multiple steps, such as pre-modification of graphene or further treatment of the as-prepared G/NPs [34,35], and NPs prepared by these methods usually do not have the desired size and morphology [36–38]. Recently, the polyol method has been used to overcome the numerous challenges related to the synthesis of NPs for electrocatalysis, and polyol methods have been shown to be effective for generating NPs and nanoalloys in a short period.

In this work, a simple one-step polyol method was used to prepare reduced graphene oxide (RGO, for simplicity graphene (G))-supported PtNi alloy NPs (G/Pt_x-Ni_{100-x}) with different component ratios. The reduction of Pt(IV), Ni(II) and GO to graphene and a dispersion of Pt–Ni NPs on graphene was simultaneously achieved in ethylene glycol, which acts as a reducing agent and solvent. Compared to a multi-step method, this method is greener, safer and more convenient because of its simple process and low cost. The hot injection method used in the NP synthesis resulted in homogeneous atomic-scale mixing of Pt and Ni within the PtNi NPs and prevented significant segregation of Pt on the surface of the NPs, which allowed for a better correlation between the NP composition (surface and bulk) and catalytic activity. The electrocatalytic activity of these G/Pt_x-Ni_{100-x} catalysts towards the MOR was investigated in both acidic and alkaline media using cyclic voltammetry (CV) and chronoamperometry (CA) analyses. Alloying Pt with Ni dramatically enhanced the electrocatalytic activity of Pt (4-6-fold increase) in both acidic and alkaline media, and the Pt_{54}–Ni_{46} composition showed the highest catalytic activity. Furthermore, a 6-8-fold increase in the catalytic activity was observed in alkaline media compared to that observed in acidic media. The CA results showed a dramatic improvement in Pt tolerance to CO poisoning after alloying Pt with Ni, and the Pt in the Pt_xNi_y alloys showed 3-5-fold higher currents in acidic media and 12-55-fold higher currents in basic media relative to pure Pt. This significant enhancement in both activity and stability is believed to be due to the Ni and RGO bi-functional effects, which are expected to be more significant in alkaline media.

2. Experimental procedures

2.1. Preparation of graphene oxide (GO)

GO was prepared by chemical oxidation of graphite powder (<20 μm, Sigma-Aldrich) using a modified Hummer's method [39]. First, in a conical flask within an ice bath, 2 g graphite powder, 1 g $NaNO_3$ (S d fine-Chem Limited, India), and 140 ml concentrated H_2SO_4 (99%, Sigma-Aldrich) were mixed and stirred for 20 min. Then, 6 g of $KMnO_4$ (S d fine-Chem Limited, India) was gradually added into the mixture with continuous stirring over 15 min followed by stirring for 1 h at 35 °C to obtain a black-green suspension. Distilled water (92 ml) was slowly added, and the temperature was increased to 98 °C. The mixture was maintained at this temperature for 30 min, ensuring complete oxidation of graphite to graphite oxide. The reaction was terminated by adding 260 ml of distilled water and 20 ml of a 30% H_2O_2 solution (LOBA Chemie, India). The change in the solution colour from black-green to brilliant yellow indicated the oxidation of pristine graphite to graphite oxide. After graphite oxidation, the mixture was washed with 600 ml of 10% HCl to remove metal ions. Finally, the product was repeatedly washed with distilled water until a neutral pH (pH 7) was obtained, and the sample of graphite oxide was collected after drying in air. To generate GO sheets, the as-obtained graphite oxide was re-dispersed in distilled water and exfoliated by ultrasonication for 30 min.

2.2. Preparation of graphene-supported Pt–Ni (G/Pt_x-Ni_y)

Three different RGO-supported Pt_xNi_y alloy NP (G/Pt_xNi_y) catalysts with different Pt:Ni atomic ratios (x:y equal 75:25, 54:46, and 40:60) were synthesized by a simple one-step polyol method. In this method, 80 mg of prepared GO was dispersed in 80 ml of ethylene glycol (EG, 99%, S d fine-Chem Limited, India) by sonication for 90 min, followed by the addition of 1 ml of a 2 M NaOH/EG solution to adjust the pH to 11. The solution was then heated under continuous stirring and refluxed in a three-neck flask at 190 °C for 2 h. To obtain NPs with a homogeneous composition and small size, a hot injection method was used as illustrated in Scheme 1. The required amounts of $H_2PtCl_6{\cdot}xH_2O$ (≥99.9%, Sigma-Aldrich) and $Ni(NO_3)_2{\cdot}6H_2O$ (98–102%, Bio Basic INC., Canada) were dissolved in 20 ml EG and injected dropwise into the previously heated solution, keeping the solution under reflux for another 2 h. Nitrogen bubbling was maintained throughout the synthesis. To collect the catalysts, the solution was allowed to cool to room temperature and then centrifuged and washed with acetone several times. Finally, the sample was dried at 80 °C in air. For comparison, graphene-supported Pt (G/Pt)

was prepared by the same method without the addition of $Ni(NO_3)_2{\cdot}6H_2O$.

2.3. Electrochemical measurements

A conventional three-electrode cell was used to carry out the electrochemical measurements with a glassy carbon (GC) electrode (5 mm in diameter) as the working electrode. Before use, the GC electrode was polished with 0.3 μm alumina to create a mirrored surface. For the acidic medium experiments, the catalyst ink was prepared by dispersing 2 mg of the catalyst powder in 0.5 ml of a diluted Nafion solution consisting of 10: 20: 70 vol % of Nafion® 117 (5%, Sigma-Aldrich): ethanol: H_2O, respectively. For the alkaline medium experiments, 2.5 mg of the catalyst powder was suspended in 0.5 ml of the diluted Nafion solution. The catalyst film was cast by drop coating 5 μL of the catalyst ink onto the surface of the GC electrode, drying the electrode at 60 °C for 10 min, and allowing it to cool down. A Pt wire and Ag/AgCl electrode (3 M KCl) were used as the counter and reference electrodes, respectively.

CV and CA were used to investigate the electrocatalytic activity and stability (tolerance to CO poisoning) of the G/Pt_xNi_y catalysts for the MOR in both acidic (0.5 M H_2SO_4) and alkaline (1 M KOH) solutions at room temperature. In the acidic medium, a potential range of - 0.2 to 1.3 V vs. Ag/AgCl and a scan rate of 20 mV/s were used, while in the alkaline medium, a potential range of −1 to 0.5 V vs. Ag/AgCl and a scan rate of 50 mV/s were applied. The electrolyte was de-aerated before each experiment by purging it with N_2 gas for approximately 30 min, and N_2 gas flowed over the solution during the measurements.

2.4. Physical characterization

The crystal structure of the prepared catalysts was examined by XRD (XPERT- PRO- PANalytical) with Cu Kα radiation (λ = 1.54 A°) in the 2θ range of 20–80°. The dispersal and size of the NPs were confirmed by HRTEM (JOEL (JEM-2100)), and the microscope operated at an acceleration voltage of 120 keV. For the TEM analysis, the catalysts were dispersed in ethanol and sonicated for 30 min before deposition onto a carbon-coated copper grid and drying before analysis. The composition of the Pt_xNi_y nanostructures on graphene was analysed by energy-dispersive X-ray spectroscopy (EDX), which was performed on a scanning electron microscope (FESEM-Zeiss SEM Ultra-60). The metal loading was confirmed by TGA (SDT Q600 V20.5 Build 15) in the temperature range of 25–800 °C at a rate of 20 °C/min under air.

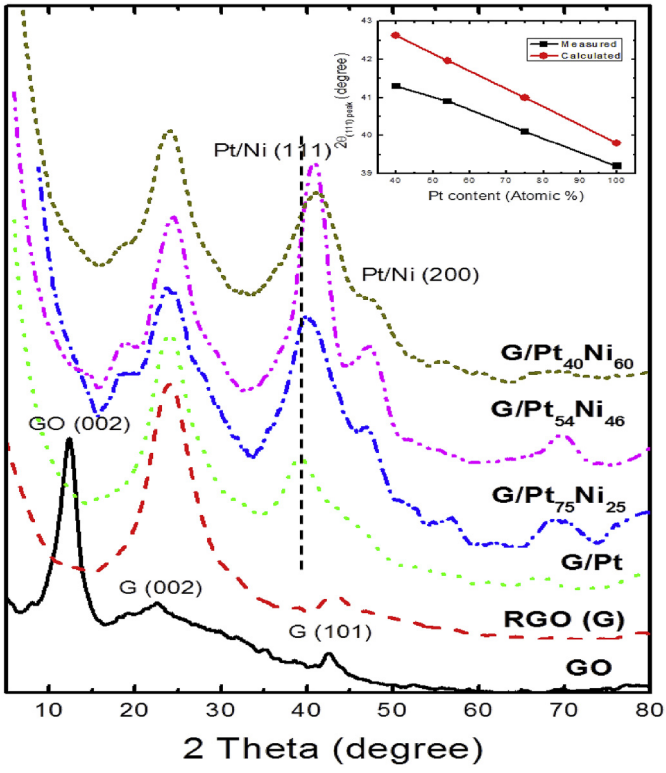

Fig. 1. XRD analysis of GO, G/RGO, G/Pt, G/Pt_{75}–Ni_{25}, G/Pt_{54}–Ni_{46}, and G/Pt_{40}–Ni_{60} catalysts.

Table 1
Chemical composition and size of the electrocatalysts.

Catalyst	XRD crystallite size (nm)	TEM particle size (nm)	Composition (at. %) by EDX (Pt:Ni)
G/Pt	1.54	3	–
G/Pt_{75}–Ni_{25}	0.6	–	74.9: 25.1
G/Pt_{54}–Ni_{46}	1.3	2.75	54.2: 45.8
G/Pt_{40}–Ni_{60}	0.7	–	39.8: 60.2

3. Results and discussion

3.1. Structural characterization

XRD patterns of the as-synthesized GO, RGO (named graphene (G) for simplicity), G/Pt, and G/Pt_xNi_y materials are given in Fig. 1. The diffraction peak of the (002) facet of GO disappeared in the patterns of all the G/Pt_xNi_y samples and was replaced with a diffraction peak at ~ 24° related to the (002) facet of graphene, indicating the successful reduction of GO to RGO [40], using the same conditions used for the NP synthesis. This result is also clearly seen for the blank sample of RGO (G). For G/Pt, the diffraction peak at a 2θ value of ~ 39.7° and the broad peaks at ~ 46.1° and ~ 67.5° correspond to the (111), (200) and (220) facets, respectively, of the Pt face-centred cubic (fcc) crystal structure. In the pattern of G/Pt_xNi_y, the Pt diffraction peaks shifted to higher 2θ values in comparison to those of G/Pt, indicating the Pt fcc lattice contracted after the introduction of Ni atoms. This behaviour and the absence of Ni diffraction peaks indicate the formation of Pt_xNi_y alloy NPs [41]. The average crystalline size of all catalysts is less than 1.5 nm, as calculated from the Debye-Scherrer equation and shown in Table 1.

Alloying degrees of the G/Pt_xNi_y are also calculated by XRD using Vegard's law [42,43]. According to the law, in the XRD pattern of G/Pt_xNi_y, the Pt (220) peak was selected for the determination of lattice parameter because the peak was far from the background signal of graphene support. The lattice parameter ($a_{(220)}$) of G/Pt_xNi_y is obtained through the equation (1) [44].

$$a_{(220)} = 2^{0.5}\lambda_{k\alpha}/\sin\theta_{max} \quad (1)$$

Where $\lambda_{k\alpha}$ is the wavelength of Cu Kα radiation and θ_{max} is the Pt (220) peak position.

In sequentially, the alloying degrees of G/Pt_xNi_y were expressed as a function of (i) Pt atomic fraction (X_{Pt}) in the G/Pt_xNi_y and (ii) nominal Pt/Ni atomic ratio ((Pt/Ni)nom) that were attained by the lattice parameter and the EDX measurement, respectively, with the following equations [45].

$$a_{(220)} = 3.8013 + 0.124X_{pt} \quad (2)$$

Table 2
Pt(220) peak position, atomic fraction of Pt in G/Pt_xNi_y and alloying degree of the G/Pt_xNi_y.

Catalyst	2θ	$a_{(220)}$	X_{pt}	alloying degree
G/Pt_{75}–Ni_{25}	68.93	3.85	0.39	22%
G/Pt_{54}–Ni_{46}	69.86	3.78	0.25	27%
G/Pt_{40}–Ni_{60}	68.5	3.82	0.227	43%

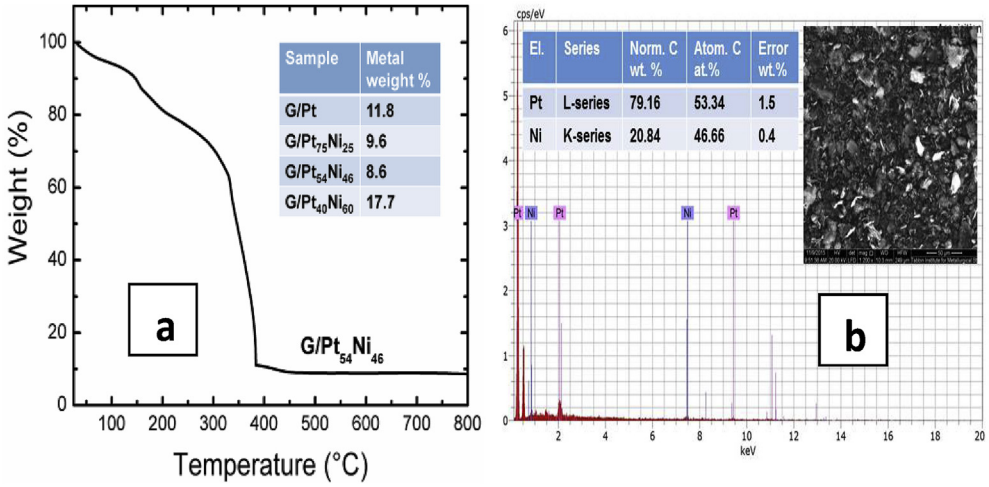

Fig. 2. (a) TGA curve of the G/Pt_{54}–Ni_{46} catalyst, (b) EDX spectrum of the G/Pt_{54}–Ni_{46} catalyst and its SEM image at a magnification of 1200×.

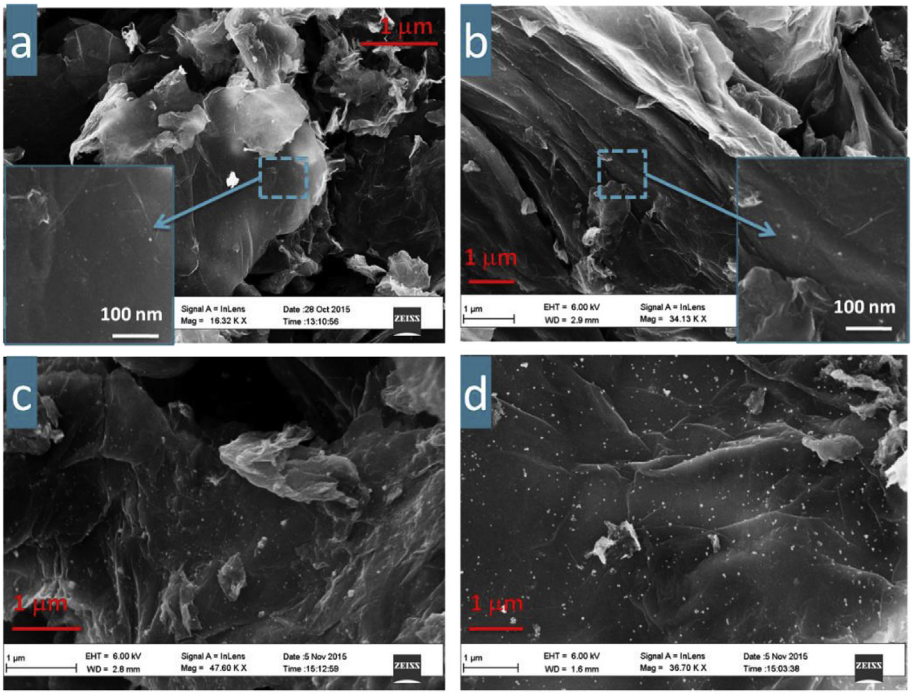

Fig. 3. HR-SEM images of the (a) G/Pt, (b) G/Pt_{75}–Ni_{25}, (c) G/Pt_{54}–Ni_{46}, and (d) G/Pt_{40}–Ni_{60} catalysts. The inset images are 10× magnification of (a) and (b).

$$\text{Alloying degree} = X_{pt} \,/\, \left(1 - X_{pt}\right)(\text{Pt/Ni})\text{nom} \quad (3)$$

Table 2 summarizes Pt(220) peak position, atomic fraction of Pt in G/PtxNiy and alloying degree of the G/Pt_xNi_y. As a result, alloying degrees of G/Pt_{75}–Ni_{25}, G/Pt_{54}–Ni_{46}, and G/Pt_{40}–Ni_{60} are 22, 27 and 43%, respectively.

The total metal loading of the prepared G/Pt and G/Pt–Ni electrocatalysts was determined by TGA, as illustrated in Fig. 2 (a). The metal

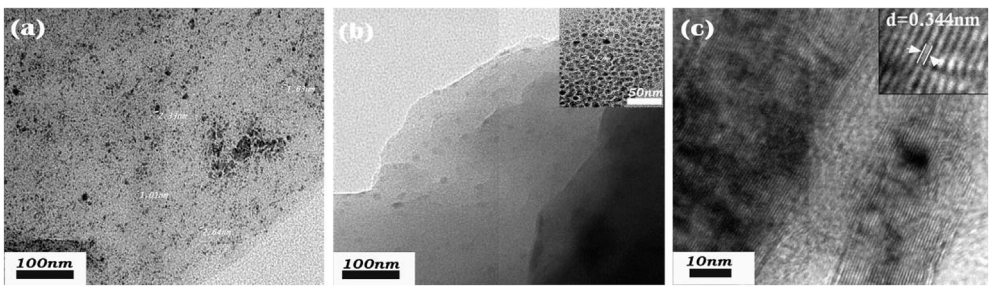

Fig. 4. HR-TEM images of (a) G/Pt and (b) G/Pt_{54}–Ni_{46} catalysts; the inset image is at a higher magnification with a scale of 50 nm (c) d-spacing of G/Pt.

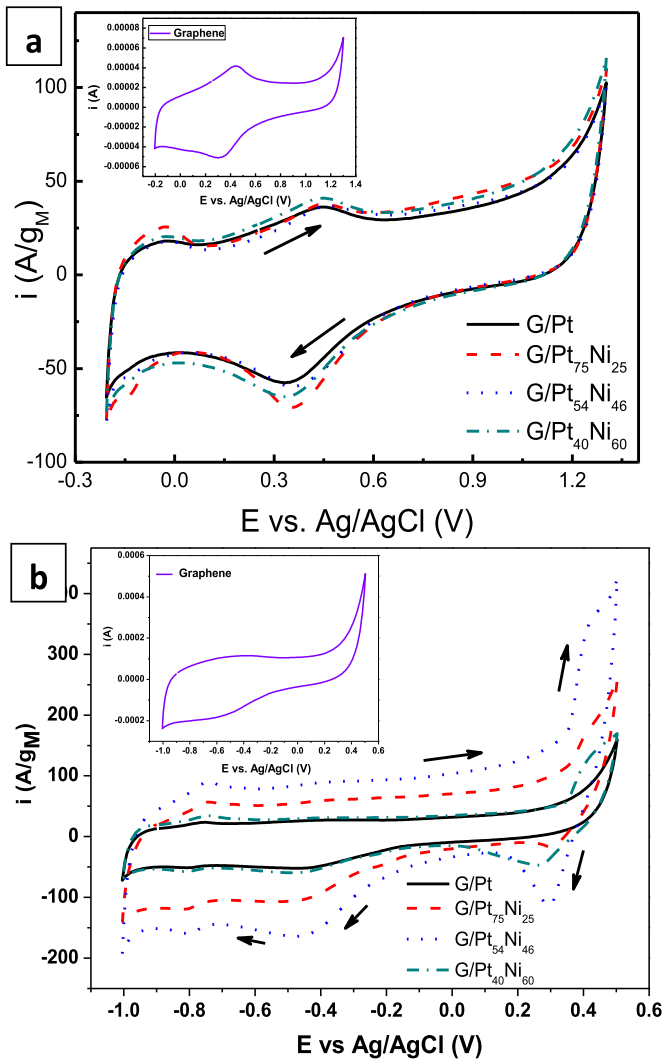

Fig. 5. (a) CV curves of G/Pt, G/Pt_{75}–Ni_{25}, G/Pt_{54}–Ni_{46}, and G/Pt_{40}–Ni_{60} catalysts in 0.5 M H_2SO_4 at a scan rate of 20 mV/s; (b) CV in 1 M KOH at a scan rate of 50 mV/s, the current was normalized to the total metal loading. The inset image is the CV of graphene under the same conditions.

loading was found to be lower than the theoretical loading (20 wt. %), which could be due to the high pH used during preparation. The high pH could result in a negatively charged graphene surface, which may restrict the adsorption of negatively charged platinum ions ($PtCl_6^{2-}$) or even negatively charged NPs after their reduction due to charge repulsion [46–48].

The composition of the nanocatalysts was analysed and confirmed by EDX analysis. Fig. 2 (b) shows the EDX spectrum of the G/Pt_{54}–Ni_{46} catalyst as an example. The Pt: Ni atomic ratios obtained by the EDX analysis for all catalysts are listed in Table 1. The ratios are nearly the same as those of the precursors involved in the reaction mixtures, indicating complete reduction of the precursors under the proposed experimental conditions.

Fig. 3 shows the HR-SEM images of the (a) G/Pt, (b) G/Pt_{75}–Ni_{25}, (c) G/Pt_{54}–Ni_{46}, and (d) G/Pt_{40}–Ni_{60} catalysts. The Pt–Ni NPs appear as light dots on dark graphene sheets, showing the uniform distribution of the Pt–Ni NPs on the graphene support. However, TEM can provide a better resolution.

Fig. 4a and b shows the HR-TEM images of the G/Pt and G/Pt_{54}–Ni_{46} as-prepared catalysts, respectively. The Pt and Pt–Ni NPs are highly homogeneous and well dispersed on the graphene support without the use of a surfactant or other additives. This uniform dispersal of NPs may be due to the effect of using EG, which prevents the agglomeration of NPs and restacking of graphene sheets [49]. Additionally, the presence of surface functional groups on the GO surface or defects in the RGO (G) may also enhance NP dispersal because these sites can act as nucleation sites.

The average particle size measured by TEM is approximately 3 nm (Table 1), which is much lower than that obtained by Habibi and Ghaderi [50], who prepared an unsupported Ni@Pt core-shell electrocatalyst (20–30 nm) using $NaBH_4$ as a reducing agent. Furthermore, PtNi/MWCNT electrocatalysts with different ratios prepared by a hydrothermal method exhibited particle size values of 6–13 nm [51].

3.2. Electrochemical characterization of the G/Pt and G/Pt_xNi_y catalysts

3.2.1. Acidic media

Fig. 5(a) depicts the cyclic voltammograms of the synthesized G/Pt and G/Pt_xNi_y catalysts in 0.5 M H_2SO_4 measured at a scan rate of 20 mV/s in the potential window of −0.2–1.3 V. The imbedded figure is the CV curve for the graphene support. The CV curves show anodic and cathodic peaks in the range of 0.3–0.6 V and 0.2–0.5 V, which are related to the oxidation and reduction of graphene, respectively. The characteristic features of Pt, including the formation and reduction of Pt oxide that appear at 0.6–0.8 V and 0.3–0.6 V in the positive and negative scans, respectively, are not present. The absence of Pt features may be because the support has a high current and the smaller Pt peaks may be imbedded in the graphene peaks. However, in the region of −0.2-0.1 V, the hydrogen under potential deposition (Hupd) peaks from polycrystalline Pt are clearly observed [52].

3.2.2. Alkaline media

Fig. 5(b) shows the CV curve of G/Pt_x-Ni_{100-x} in a N_2-saturated 1 M KOH solution at a scan rate of 50 mV/s in the potential range from −1 V to 0.5 V. The hydrogen adsorption/desorption peaks were observed in the potential region from −0.9 to −0.7 V in the anodic and cathodic scans [50]. The anodic broad peak at potential values from −0.6 to −0.3 V may be related to the formation of Pt(II) oxide (PtO) species. Although the oxidation process is still not clearly understood, it is well accepted that the OH^- ions are chemisorbed in the initial step of oxide formation [53]. The oxidation reaction mechanism may be explained by the combination of reactions 1 and 2 or 1 and 3 [54]:

$$Pt + OH^- \rightarrow Pt(OH)_{ads} + e^- \quad (1)$$

$$Pt(OH)_{ads} + OH^- \rightarrow PtO + H_2O + e^- \quad (2)$$

$$2Pt(OH)_{ads} \rightarrow PtO + Pt + H_2O \quad (3)$$

Due to the presence of Ni in the G/Pt_xNi_y electrocatalysts, a distinct peak was observed, indicating more facile formation of surface oxides, which plays an important part in improving the CO tolerance of the synthesized electrocatalysts. The dominant reduction peak of the Pt oxide species was seen for all electrocatalysts in the cathodic scan in the same region (−0.6 to −0.3 V).

Two other peaks, which were absent in the CV curve of G/Pt, were also observed for all G/Pt_x-Ni_{100-x} electrocatalysts at potential values of approximately 0.4 V and 0.3 V in the anodic and cathodic direction, respectively. These peaks were due to the formation of NiOOH species in alkaline solution via reactions 4 and 5 [55]:

$$Ni + 2OH^- \rightarrow Ni(OH)_2 + 2e^- \quad (4)$$

$$Ni(OH)_2 + OH^- \rightarrow NiOOH + H_2O + e^- \quad (5)$$

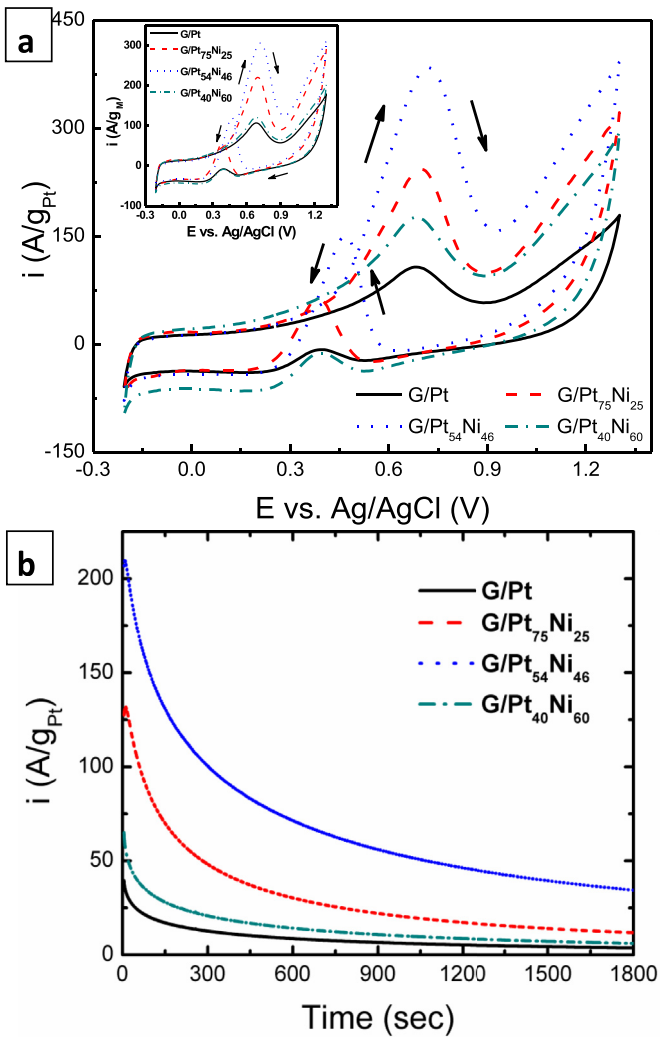

Fig. 6. (a) Mass activity of the G/Pt, G/Pt_{75}–Ni_{25}, G/Pt_{54}–Ni_{46}, and G/Pt_{40}–Ni_{60} catalysts in 0.5 M H_2SO_4 containing 1 M CH_3OH at a scan rate of 20 mV/s; the current was normalized to the Pt loading or the total metal loading in the inset. (b) Amperometry results (i-t curves) at 0.6 V.

3.3. The electrocatalytic activity of G/Pt and G/Pt_xNi_y catalysts for the MOR

3.3.1. Acidic media

The electrocatalytic performance of the G/Pt and G/Pt_xNi_y catalysts for the MOR is shown in Fig. 6(a). The anodic peak at ~ 0.7 V in the forward scan and the peak at ~ 0.4 V in the reverse scan are related to the MOR occurring at previously poisoned and clean surfaces, respectively. In the forward scan, carbonaceous poisoning intermediates, such as CO, block the surface and prevent further methanol oxidation at low potentials (reaction 6). At high potentials, water dissociation occurs (reaction 7), which allows oxidation of adsorbed CO and frees the Pt surface (reaction 8) for further methanol oxidation [35,56].

$$Pt + CH_3OH \rightarrow Pt(CO)_{ads} + 4H^+ + 4e^- \quad (6)$$

$$M + H_2O \rightarrow M(OH)_{ads} + H^+ + e^- \quad (7)$$

$$Pt(CO)_{ads} + M(OH)_{ads} \rightarrow Pt + M + CO_2 + H^+ + e^- \quad (8)$$

In the reverse scan, the MOR takes place on a clean surface because the poisonous species on the surface are removed at high potentials. At high potentials, Pt has an oxide layer that is not as active as metallic Pt, resulting in the current peaks in the forward scan. A methanol oxidation current is observed in the reverse scan once a portion of this oxide layer is converted to metallic Pt. The onset potential and peak current in the reverse scan depend on the reduction of Pt oxide.

As illustrated in Fig. 6(a), G/Pt_{54}–Ni_{46} exhibits the highest mass activity (260 A/g_{Pt}), which is three times greater than that of G/Pt (85 A/g_{Pt}). The other two catalysts containing Ni, G/Pt_{75}–Ni_{25} and G/Pt_{40}–Ni_{60}, have catalytic activities 2 and 1.6 times higher than that of G/Pt. The current density according to the total metal loading also has the same trend. G/Pt_{75}–Ni_{25}, G/Pt_{54}–Ni_{46}, and G/Pt_{40}–Ni_{60} have mass activities of 168, 219, and 99 A/g_M, which are 2, 2.6, and 1.2 times higher, respectively, than that of G/Pt (85 A/g_M). The current density values were calculated at a constant potential of 0.6 V and are listed in Table 3. It is worthy to mention that the obtained mass activity for G/Pt_{54}–Ni_{46} electrocatalyst (260 A/g_{Pt}) is much higher than those reported for Pt_1–Ni_1 nanohybrids prepared by Polyol Process (136 mA/mg_{Pt}) [57], Pt_3–Ni_1/G prepared by Galvanic Replacement (214 mA/mg_{Pt}) [49], and Chemical Co-reduction of Ni@Pt/MWCNTs (183 mA/mg_{Pt}) [58].

The MOR happens via methanol adsorption, successive dehydrogenation into intermediates (e.g., CO) and then oxidation of CO to CO_2 [59,60]. Pt activates the C–H bond, allowing cleavage of adsorbed methanol. Then, Pt–CO species form and are strongly adsorbed on the Pt surface, blocking the active sites for methanol adsorption and restricting methanol oxidation.

The methanol adsorption/dehydrogenation step in the MOR requires three neighbouring Pt atoms. When alloying Pt with Ni, e.g., in the sample G/Pt_{75}–Ni_{25}, Ni atoms insert into the Pt lattice and nickel hydroxide forms in the medium, producing OH species to remove the intermediate CO and free the Pt active sites for methanol adsorption [61,62]. Upon increasing the Ni content to G/Pt_{54}–Ni_{46}, the activity of the catalyst for the MOR increased because the rate of generating OH increases and some Pt active sites are not covered by Ni. In the G/Pt_{40}–Ni_{60} catalyst, the activity decreased, which is possibly because the excess Ni covered the surface active sites of Pt that are responsible for methanol adsorption, resulting in an overall decrease in the rate of the MOR.

All catalysts containing Ni exhibited the same onset potential, i.e., ~ 0.27 V (vs. Ag/AgCl), which is a negative shift of ~ 80 mV compared with that of G/Pt (~ 0.35 V). This shift suggests a higher catalytic activity and that the MOR can more easily proceed on the surface of catalysts containing Ni than G/Pt. We determined the onset potential values at a constant current density of 2 A/g_{Pt}.

The stability of the catalysts was tested by amperometry under a constant potential of 0.6 V for 1800 s (Fig. 6(b)). The high primary current was mainly related to double-layer charging. All catalysts displayed rapid current decreases in the initial stage due to the formation of intermediate species, such as CO_{ads} and CHO_{ads}, during the MOR [63]. However, the anodic current density of the G/Pt_{54}–Ni_{46} nanocatalyst was

Table 3
Comparison of the electrochemical activities of the catalysts in acidic media.

Electrochemical activities of the catalysts in acidic media					
Catalyst	Pt Content (g/cm^2)	Mass activity (A/g_{Pt})	Mass activity (A/g_M)	Peak potential (V)	Onset potential (V)
G/Pt	1.2E-5	85	85	0.68	0.35
G/Pt_{75}–Ni_{25}	9.2E-6	176	168	0.7	0.27
G/Pt_{54}–Ni_{46}	5.9E-6	260	219	0.72	0.27
G/Pt_{40}–Ni_{60}	9E-6	141	99	0.68	0.27

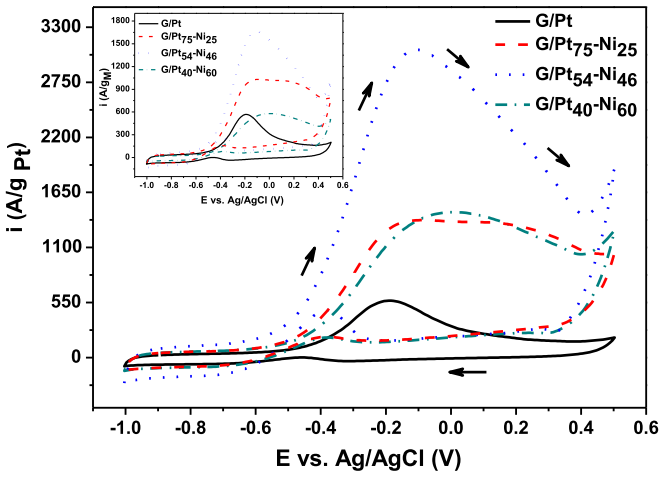

Fig. 7. Mass activity of the G/Pt, G/Pt_{75}–Ni_{25}, G/Pt_{54}–Ni_{46}, and G/Pt_{40}–Ni_{60} catalysts in 1 M KOH containing 1 M CH_3OH at a scan rate of 50 mV/s; the current was normalized to the Pt loading content or the total metal loading in the inset.

the highest during the initial time period, indicating that G/Pt_{54}–Ni_{46} has excellent electrocatalytic stability for the MOR.

3.3.2. *In alkaline media*

The electrocatalytic activity of different G/Pt_x-Ni_{100-x} electrocatalysts for the MOR is depicted in Fig. 7. Cyclic voltammograms were obtained in a 1 M KOH +1 M methanol solution at 50 mV/s. For the G/Pt electrocatalyst, the peak in the forward scan (anodic direction) related to methanol oxidation appeared in the potential range from −0.4 V to 0.0 V. In the presence of Ni, the peak was broader and covered a wider potential range from −0.5 V to 0.4 V with a higher current density. Additionally, the peak in the reverse scan, which was observed in the potential range from −0.6 V to −0.4 V for G/Pt and from −0.6 V to −0.3 V for G/Pt_x-Ni_{100-x}, may be due to the oxidation of intermediates and CO species, similar to the results observed in acidic media [64]. The peak currents for G/Pt_x-Ni_{100-x} in the anodic and cathodic scans shifted to more positive potential values than those of G/Pt. Furthermore, higher methanol oxidation current density values at lower potentials were achieved for all G/Pt_x-Ni_{100-x} electrocatalysts .

The enhanced mass activity according to Pt loading can be arranged in ascending order as follows: G/Pt (566 A/g_{Pt}) < G/Pt_{40}–Ni_{60} (1091 A/g_{Pt}, 1.93 times) < G/Pt_{75}–Ni_{25} (1252 A/g_{Pt}, 2.21 times) < G/Pt_{54}–Ni_{46} (2732 A/g_{Pt}, 4.83 times). For the total metal loading, the order is different: G/Pt_{40}–Ni_{60} (441 A/g_M) < G/Pt (566 A/g_M) < G/Pt_{75}–Ni_{25} (951 A/g_M) < G/Pt_{54}–Ni_{46} (1491 A/g_M). The current density was calculated at a constant potential of −0.2 V (see Table 4). Note that the activity of the optimum composition (G/Pt_{54}–Ni_{46}) is much higher than those reported for Pt_7–Ni_3/C_x which prepared by Incipient Wetness (29 A/g_{Pt}) [65], Pt_3Ni_1/C obtained through by Polyol Process (559 mA/mg_{Pt}) [52], Pt_3Ni_1/C by Polyol Process (0.414 A/mg_{Pt}) [66], and Chemical Co-reduction of Ni@Pt/MWCNTs (284 mA/mg_{Pt}) [66]. As the amount of Ni increased from G/Pt_{75}–Ni_{25} to G/Pt_{54}–Ni_{46}, the current density increased; however, an excess of Ni (G/Pt_{40}–Ni_{60}) led to detrimental effects, as observed in acidic media.

The G/Pt_{40}–Ni_{60} electrocatalyst showed a low current density, which may be attributed to the conversion of Ni into NiO/$Ni(OH)_2$, which then covers Pt atoms in the polarization process [57]. Additionally, as the number of oxidation products increases, intermediate oxidation products may adsorb on the catalyst surface and restrict further methanol oxidation [68].

More negative onset potential values were observed for all studied G/Pt_x-Ni_{100-x} electrocatalysts compared to those of G/Pt, as illustrated in Fig. 8(a). The G/Pt_{75}–Ni_{25} and G/Pt_{40}–Ni_{60} catalysts have the same onset

Table 4
Comparison of the electrochemical activities of the catalysts in alkaline media.

Electrochemical activities of the catalysts in alkaline media						
Catalyst	Pt Content (g/cm^2)	Mass activity (A/g_{Pt})	Mass activity (A/g_M)	Current density (A/g_{Pt}) after 3600 s from CA	Peak potential (V)	Onset potential (V)
G/Pt	1.2E-5	566	566	16	−0.19	−0.4
G/Pt_{75}–Ni_{25}	9.2E-6	1252	951	130	−0.1	−0.45
G/Pt_{54}–Ni_{46}	5.9E-6	2732	1491	543	−0.1	−0.5
G/Pt_{40}–Ni_{60}	9E-6	1091	441	160	0.0	−0.45

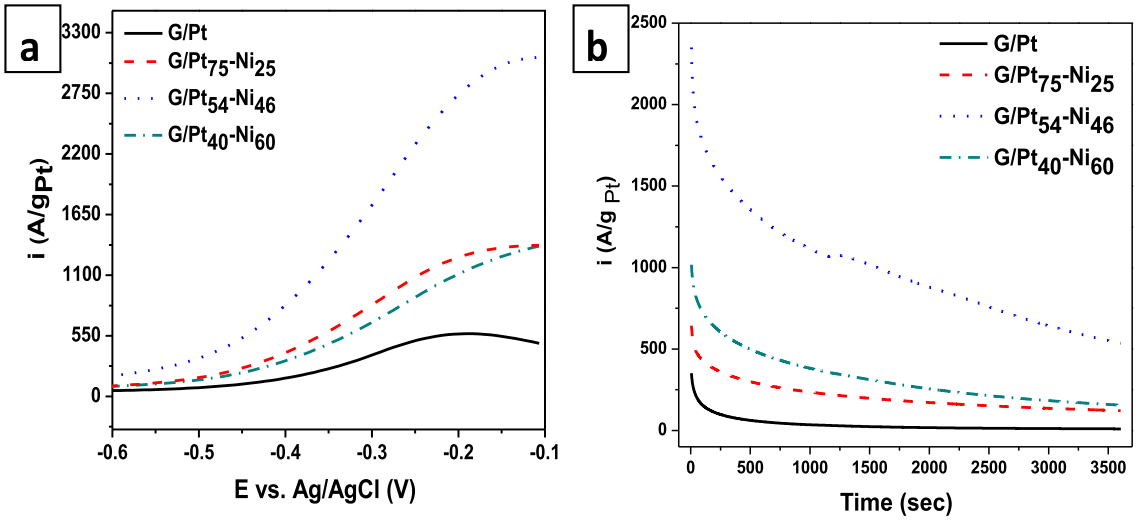

Fig. 8. (a) The activity of all catalysts in 1 M KOH + 1 M CH_3OH at a scan rate of 50 mV/s in the potential range from −0.6 to −0.1 V to show the onset potential. (b) CA i-t curves at −0.2 V.

potential, −0.45 V, while G/Pt_{54}–Ni_{46} has an onset potential of −0.5 V, which represent negative shifts of 50 mV and 100 mV, respectively, compared to the potential of G/Pt (−0.4 V), as shown in Table 4. The lower onset potentials of all catalysts containing Ni indicate their enhanced electrocatalytic activity and kinetics for the MOR.

CA is an effective method to evaluate the electrocatalytic activity and stability of catalyst materials [69]. Fig. 8(b) shows the current density-time responses of all G/Pt_x-Ni_{100-x} electrocatalysts for methanol electrooxidation at a constant potential value (−0.2 V vs Ag/AgCl). All catalysts showed a gradual current decay before a steady current status was attained, and the gradual decay was attributed to the formation of some Pt (and/or Ni) oxides/hydroxides and other adsorbed intermediates during the MOR [70,71]. As predicted, the methanol oxidation current of the electrocatalysts containing Ni was higher than that of G/Pt. After 3600 s, G/Pt_{75}–Ni_{25}, G/Pt_{40}–Ni_{60} and G/Pt_{54}–Ni_{46} presented current densities of 130, 160 and 543 A/g_{Pt}, respectively, which are 8, 10 and 34 times higher than that of G/Pt (16 A/g_{Pt}). In summary, the results indicate that the G/Pt_{54}–Ni_{46} electrocatalyst has the highest overall electrocatalytic activity among the four electrocatalysts.

The improved catalytic activity of the G/Pt_x-Ni_{100-x} nanocatalysts can be attributed to the synergistic effect of Pt and Ni in the catalysts and the change in the electronic properties of Pt, which occurs due to the existence of Ni in the catalysts. The geometric environment and atomic configuration of the Pt atoms in Pt–Ni catalysts change owing to the formation of an alloy with Ni. This change may affect the electronic structure of Pt [57,72], leading to an alteration in the electrocatalytic activity for the MOR. Another study showed that when Ni was alloyed with Pt, the electronic structure of Pt is modified because of charge transfer from Ni to Pt, which lowers the density of states at the Fermi level [73], reduces the Pt–CO bond energy, and weakens CO adsorption on Pt–Ni catalysts [74]. Therefore, the electrocatalytic activity of the G/Pt_x-Ni_{100-x} nanocatalysts is improved.

It is clear that the activity and stability of all catalysts are greater in alkaline media than acidic media because methanol was almost completely oxidized in the alkaline medium during the forward scan compared to incomplete oxidation in the acidic medium [75,76]. The explanation for this difference is the presence of a large amount of free OH^- ions, which might also contribute to this reaction via the Eley–Rideal mechanism [77], and the high stability of less noble metals in alkaline media.

4. Conclusion

In summary, a facile and modified polyol method has been developed to disperse Pt–Ni NPs on graphene sheets. Graphene can be used as an ideal substrate for growing and anchoring Pt–Ni NPs with a very narrow size distribution. The reduction of GO to graphene and doping of Pt–Ni NPs on graphene were simultaneously performed in EG. The synthesized Pt–Ni alloy NPs supported on graphene sheets were highly dispersed, and the particle size was approximately 1–3 nm without a surfactant. The electrochemical activities were investigated by CV and CA in acidic and alkaline media and showed promising results. The G/Pt_{75}–Ni_{25}, G/Pt_{54}–Ni_{46} and G/Pt_{40}–Ni_{60} catalysts showed higher mass activities than G/Pt in both acidic and alkaline media. The catalytic activity in alkaline media is higher than that for acidic media by approximately 10 times. The G/Pt_{54}–Ni_{46} catalyst showed the highest electrocatalytic activity (260 A/g_{Pt} in acidic media and 2732 A/g_{Pt} in alkaline media) and stability for the MOR and better tolerance of intermediate species; accordingly, this catalyst is favoured for long-term application as an anode material for DMFCs.

Acknowledgements

The facilities and financial support of the present work by the National Research Centre and the American University in Cairo are highly appreciated.

References

[1] M.A. Abdelkareem, E.T. Kasem, N. Nakagawa, E.A.M. Abdelghani, A.A. Elzatahry, K.A. Khalil, et al., Enhancement of the passive direct methanol fuel cells performance by modification of the cathode microporous layer using carbon nanofibers, Fuel Cells 14 (2014) 607–613, https://doi.org/10.1002/fuce.201300279.
[2] R. Abdullah Mirzaie, A. Eshghi, Study of methanol electro-oxidation on Ni and Ni–Pt/carbon paper electrodes for direct methanol fuel cell applications, Surf. Eng. 30 (2014) 263–267, https://doi.org/10.1179/1743294414Y.0000000248.
[3] Y.C. Shi, L.P. Mei, A.J. Wang, T. Yuan, S.S. Chen, J.J. Feng, L-Glutamic acid assisted eco-friendly one-pot synthesis of sheet-assembled platinum-palladium alloy networks for methanol oxidation and oxygen reduction reactions, J. Colloid Interface Sci. 504 (2017) 363–370, https://doi.org/10.1016/j.jcis.2017.05.058.
[4] N.a.M. Barakat, M. Motlak, M.M. Nassar, Abdelkareem M a, M.S. Mahmoud, M.H. El-Newehy, et al., From secondary to primary role in alkaline fuel cells: Co-decorated graphene as effective catalyst for ethanol oxidation, ECS Electrochem Lett 4 (2014) F5–F8, https://doi.org/10.1149/2.0011401eel.
[5] R. Singh, R. Awasthi, C. Sharma, Review : an overview of recent development of platinum- based cathode materials for direct methanol fuel cells, Int J Electrochem Sci 9 (2014) 5607–5639.
[6] R.S. Amin, K.M. El-Khatib, S. Siracusano, V. Baglio, A. Stassi, A.S. Arico, Metal oxide promoters for methanol electro-oxidation, Int. J. Hydrogen Energy 39 (2014) 9782–9790, https://doi.org/10.1016/j.ijhydene.2014.04.100.
[7] M. Oezaslan, Hasché F, strasser P. Oxygen electroreduction on PtCo3, PtCo and Pt3Co alloy nanoparticles for alkaline and acidic PEM fuel cells, J. Electrochem. Soc. 159 (2012), https://doi.org/10.1149/2.075204jes. B394.
[8] B. Luo, S. Xu, X. Yan, Q. Xue, Graphene nanosheets supported hollow Pt&CoSn(OH)6 nanospheres as a catalyst for methanol electro-oxidation, J. Power Sources 205 (2012) 239–243, https://doi.org/10.1016/j.jpowsour.2012.01.077.
[9] E. Bertin, S. Garbarino, A. Ponrouch, D. Guay, Synthesis and characterization of PtCo nanowires for the electro-oxidation of methanol, J. Power Sources 206 (2012) 20–28, https://doi.org/10.1016/j.jpowsour.2012.01.015.
[10] E. Antolini, J.R.C. Salgado, E.R. Gonzalez, The stability of Pt-M (M = first row transition metal) alloy catalysts and its effect on the activity in low temperature fuel cells. A literature review and tests on a Pt-Co catalyst, J. Power Sources 160 (2006) 957–968, https://doi.org/10.1016/j.jpowsour.2006.03.006.
[11] B.N. Wanjala, J. Luo, R. Loukrakpam, B. Fang, D. Mott, P.N. Njoki, et al., Nanoscale Alloying, phase-segregation, and Core−Shell evolution of Gold−Platinum nanoparticles and their electrocatalytic effect on oxygen reduction reaction, Chem. Mater. 22 (2010) 4282–4294, https://doi.org/10.1021/cm101109e.
[12] S. Koh, M.F. Toney, P. Strasser, Activity–stability relationships of ordered and disordered alloy phases of Pt3Co electrocatalysts for the oxygen reduction reaction (ORR), Electrochim. Acta 52 (2007) 2765–2774, https://doi.org/10.1016/j.electacta.2006.08.039.
[13] I. Matanović, F.H. Garzon, N.J. Henson, Theoretical study of electrochemical processes on Pt–Ni alloys, J. Phys. Chem. C 115 (2011) 10640–10650, https://doi.org/10.1021/jp111930w.
[14] R. Loukrakpam, J. Luo, T. He, Y. Chen, Z. Xu, P.N. Njoki, et al., Nanoengineered PtCo and PtNi catalysts for oxygen reduction reaction: an assessment of the structural and electrocatalytic properties, J. Phys. Chem. C 115 (2011) 1682–1694, https://doi.org/10.1021/jp109630n.
[15] V. Baglio, A.S. Aric, A. Stassi, C.D. Urso, Blasi A. Di, A.M.C. Luna, et al., Investigation of Pt – Fe catalysts for oxygen reduction in low temperature direct methanol fuel cells 159 (2006) 900–904, https://doi.org/10.1016/j.jpowsour.2005.12.088.
[16] C.H. Yen, K. Shimizu, Y.Y. Lin, F. Bailey, I.F.W.C. Cheng, C.H. Yen, K. Shimizu, Y.Y. Lin, F. Bailey, I.F. Cheng, et al., Chemical fluid deposition of Pt-based bimetallic nanoparticles on multiwalled carbon nanotubes for direct methanol fuel cell application, Energy Fuels 21 (2007) 2268–2271, https://doi.org/10.1021/ef0606409.
[17] C. Xu, J. Hou, X. Pang, X. Li, M. Zhu, B. Tang, Nanoporous PtCo and PtNi alloy ribbons for methanol electrooxidation, Int. J. Hydrogen Energy 37 (2012) 10489–10498, https://doi.org/10.1016/j.ijhydene.2012.04.041.
[18] X.W. Zhou, R.H. Zhang, Z.Y. Zhou, S.G. Sun, Preparation of PtNi hollow nanospheres for the electrocatalytic oxidation of methanol, J. Power Sources 196 (2011) 5844–5848, https://doi.org/10.1016/j.jpowsour.2011.02.088.
[19] R. Xiu, F. Zhang, Z. Wang, M. Yang, J. Xia, R. Gui, et al., Electrodeposition of PtNi bimetallic nanoparticles on three-dimensional graphene for highly efficient methanol oxidation, RSC Adv. 5 (2015) 86578–86583, https://doi.org/10.1039/C5RA13728D.
[20] A.B.A.A. Nassr, I. Sinev, M.M. Pohl, W. Grünert, M. Bron, Rapid microwave-assisted polyol reduction for the preparation of highly active PtNi/CNT electrocatalysts for methanol oxidation, ACS Catal. 4 (2014) 2449–2462, https://doi.org/10.1021/cs401140g.
[21] Y. Zhao, E. Yifeng, L. Fan, Y. Qiu, S. Yang, A new route for the electrodeposition of platinum – nickel alloy nanoparticles on multi-walled carbon nanotubes, Electrochim. Acta 52 (2007) 5873–5878, https://doi.org/10.1016/j.electacta.2007.03.020.
[22] S. Kim, M.-H. Cho, J.-R. Lee, S.-J. Park, Influence of plasma treatment of carbon blacks on electrochemical activity of Pt/carbon blacks catalysts for DMFCs, J. Power Sources 159 (2006) 46–48, https://doi.org/10.1016/j.jpowsour.2006.04.039.
[23] Z.Q. Tian, S.P. Jiang, Y.M. Liang, P.K. Shen, Synthesis and characterization of platinum catalysts on multiwalled carbon nanotubes by intermittent microwave irradiation for fuel cell applications, J. Phys. Chem. B 110 (2006) 5343–5350, https://doi.org/10.1021/jp056401o.

[24] H. Yang, C. Coutanceau, J.-M. Léger, N. Alonso-Vante, Methanol tolerant oxygen reduction on carbon-supported Pt–Ni alloy nanoparticles, J. Electroanal. Chem. 576 (2005) 305–313, https://doi.org/10.1016/j.jelechem.2004.10.026.
[25] F. Zhu, G. Ma, Z. Bai, R. Hang, B. Tang, Z. Zhang, et al., High activity of carbon nanotubes supported binary and ternary Pd-based catalysts for methanol, ethanol and formic acid electro-oxidation, J. Power Sources 242 (2013) 610–620, https://doi.org/10.1016/j.jpowsour.2013.05.145.
[26] M.G. Hosseini, R. Mahmoodi, V. Daneshvari-Esfahlan, Ni@Pd core-shell nanostructure supported on multi-walled carbon nanotubes as efficient anode nanocatalysts for direct methanol fuel cells with membrane electrode assembly prepared by catalyst coated membrane method, Energy 161 (2018) 1074–1084, https://doi.org/10.1016/j.energy.2018.07.148.
[27] N.A.M. Barakat, M. Motlak, B.S. Kim, A.G. El-Deen, S.S. Al-Deyab, A.M. Hamza, Carbon nanofibers doped by NixCo1-x alloy nanoparticles as effective and stable non precious electrocatalyst for methanol oxidation in alkaline media, J. Mol. Catal. A Chem. 394 (2014) 177–187, https://doi.org/10.1016/j.molcata.2014.07.011.
[28] B. Kuppan, P. Selvam, Platinum-supported mesoporous carbon (Pt/CMK-3) as anodic catalyst for direct methanol fuel cell applications: the effect of preparation and deposition methods, Prog Nat Sci Mater Int 22 (2012) 616–623, https://doi.org/10.1016/j.pnsc.2012.11.005.
[29] J.H. Bang, K. Han, S.E. Skrabalak, H. Kim, K.S. Suslick, Porous carbon supports prepared by ultrasonic spray pyrolysis for direct methanol fuel cell electrodes, J. Phys. Chem. C 111 (2007) 10959–10964, https://doi.org/10.1021/jp071624v.
[30] Y. Hu, P. Wu, Y. Yin, H. Zhang, C. Cai, Effects of structure, composition, and carbon support properties on the electrocatalytic activity of Pt-Ni-graphene nanocatalysts for the methanol oxidation, Appl. Catal. B Environ. 111–112 (2012) 208–217, https://doi.org/10.1016/j.apcatb.2011.10.001.
[31] V. Singh, D. Joung, L. Zhai, S. Das, S.I. Khondaker, S. Seal, Graphene based materials: past, present and future, Prog. Mater. Sci. 56 (2011) 1178–1271, https://doi.org/10.1016/j.pmatsci.2011.03.003.
[32] Q. Yue, K. Zhang, X. Chen, L. Wang, J. Zhao, J. Liu, et al., Generation of OH radicals in oxygen reduction reaction at Pt-Co nanoparticles supported on graphene in alkaline solutions, Chem. Commun. 46 (2010) 3369–3371, https://doi.org/10.1039/c000084a.
[33] R.P. Antony, L.K. Preethi, B. Gupta, T. Mathews, S. Dash, A.K. Tyagi, Efficient electrocatalytic performance of thermally exfoliated reduced graphene oxide-Pt hybrid, Mater. Res. Bull. 70 (2015) 60–67, https://doi.org/10.1016/j.materresbull.2015.04.015.
[34] N. Seselj, C. Engelbrekt, J. Zhang, Graphene-supported platinum catalysts for fuel cells, Sci. Bull. 60 (2015) 864–876, https://doi.org/10.1007/s11434-015-0745-8.
[35] W. Qian, R. Hao, J. Zhou, M. Eastman, B.A. Manhat, Q. Sun, et al., Exfoliated graphene-supported Pt and Pt-based alloys as electrocatalysts for direct methanol fuel cells, Carbon N Y 52 (2013) 595–604, https://doi.org/10.1016/j.carbon.2012.10.031.
[36] H.N. Dinh, X. Ren, F.H. Garzon, Piotr Zelenay, S. Gottesfeld, Electrocatalysis in direct methanol fuel cells: in-situ probing of PtRu anode catalyst surfaces, J. Electroanal. Chem. 491 (2000) 222–233, https://doi.org/10.1016/S0022-0728(00)00271-0.
[37] Thamer El-Newehy, M.H., Barakat, N.A.M., Abdelkareem, M.A., Al-Deyab, S.S., Kim, H.Y. BM. In-situ synthesis of Ni/N-doped CNFs-supported graphite disk as effective immobilized catalyst for methanol electrooxidation, Int. J. Hydrogen Energy 40 (2015) 14845–14856, https://doi.org/10.1016/j.ijhydene.2015.08.091.
[38] R. Lin, T. Zhao, M. Shang, J. Wang, W. Tang, V.E. Guterman, et al., Effect of heat treatment on the activity and stability of PtCo/C catalyst and application of in-situ X-ray absorption near edge structure for proton exchange membrane fuel cell, J. Power Sources 293 (2015) 274–282, https://doi.org/10.1016/j.jpowsour.2015.05.067.
[39] D.C. Marcano, D.V. Kosynkin, J.M. Berlin, A. Sinitskii, Z. Sun, A. Slesarev, et al., Improved synthesis of graphene oxide, ACS Nano 4 (2010) 4806–4814, https://doi.org/10.1021/nn1006368.
[40] S.A. Elsherif, M.F. Zawrah, N.A.A. Abdel Ghany, F.A. Taher, R.M. Khattab, M.M. El-Fass, Nanoelectrocatalyst anode for direct methanol fuel cells: fabrication and electrochemical characterization of graphene/Pt-Ni, Egypt. J. Chem. 58 (2015) 459–474.
[41] A.B.A.A. Nassr, I. Sinev, W. Grünert, M. Bron, PtNi supported on oxygen functionalized carbon nanotubes: in depth structural characterization and activity for methanol electrooxidation, Appl. Catal. B Environ. 142–143 (2013) 849–860, https://doi.org/10.1016/j.apcatb.2013.06.013.
[42] C.V. Rao, A.L.M. Reddy, Y. Ishikawa, P.M. Ajayan, Synthesis and electrocatalytic oxygen reduction activity of graphene-supported Pt3Co and Pt3Cr alloy nanoparticles, Carbon N Y 49 (2011) 931–936, https://doi.org/10.1016/j.carbon.2010.10.056.
[43] D. Wang, L. Zhuang, J. Lu, An alloying-degree-controlling step in the impregnation synthesis of PtRu/C catalysts, J. Phys. Chem. C 111 (2007) 16416–16422, https://doi.org/10.1021/jp073062l.
[44] E. Antolini, F. Cardellini, Formation of carbon supported PtRu alloys: an XRD analysis, J. Alloys Compd. 315 (1–2) (2001) 118–122.
[45] K. Hyun, J.H. Lee, C.W. Yoon, Y. Kwon, The effect of platinum based bimetallic electrocatalysts on oxygen reduction reaction of proton exchange membrane fuel cells, Int. J. Electrochem. Sci. 8 (1) (2013) 11752–11767.
[46] V.A. Ribeiro, O.V. Correa, A.O. Neto, M. Linardi, E.V. Spinacé, Preparation of PtRuNi/C electrocatalysts by an alcohol-reduction process for electro-oxidation of methanol, Appl. Catal. Gen. 372 (2010) 162–166, https://doi.org/10.1016/j.apcata.2009.10.028.
[47] L. Ren, Y. Xing, Effect of pH on PtRu electrocatalysts prepared via a polyol process on carbon nanotubes, Electrochim. Acta 53 (2008) 5563–5568, https://doi.org/10.1016/j.electacta.2008.02.109.
[48] H.-S. Oh, J.-G. Oh, Y.-G. Hong, H. Kim, Investigation of carbon-supported Pt nanocatalyst preparation by the polyol process for fuel cell applications, Electrochim. Acta 52 (2007) 7278–7285, https://doi.org/10.1016/j.electacta.2007.05.080.
[49] Y. Hu, P. Wu, H. Zhang, C. Cai, Synthesis of graphene-supported hollow Pt-Ni nanocatalysts for highly active electrocatalysis toward the methanol oxidation reaction, Electrochim. Acta 85 (2012) 314–321, https://doi.org/10.1016/j.electacta.2012.08.080.
[50] S. Ghaderi, B. Habibi, Ni@Pt core-shell nanoparticles as an improved electrocatalyst for ethanol electrooxidation in alkaline media, Iran J Hydrog Fuel Cell 2 (2015) 109–119.
[51] K. Ding, Y. Zhao, L. Liu, Y. Cao, Q. Wang, H. Gu, et al., Pt–Ni bimetallic composite nanocatalysts prepared by using multi-walled carbon nanotubes as reductants for ethanol oxidation reaction, Int. J. Hydrogen Energy 39 (2014) 17622–17633, https://doi.org/10.1016/j.ijhydene.2014.08.150.
[52] Q. Jiang, L. Jiang, H. Hou, J. Qi, S. Wang, G. Sun, Promoting effect of Ni in PtNi bimetallic electrocatalysts for the methanol oxidation reaction in alkaline media: experimental and density functional theory studies, J. Phys. Chem. C 114 (2010) 19714–19722, https://doi.org/10.1021/jp1039755.
[53] S. Ghosh, A. Teillout, D. Floresyona, P. de Oliveira, A. Hagege, H. Remita, Conducting polymer-supported palladium nanoplates for applications in direct alcohol oxidation, Int. J. Hydrogen Energy 40 (14) (2015) 4951–4959, https://doi.org/10.1016/j.ijhydene.2015.01.101.
[54] Z.X. Liang, T.S. Zhao, J.B. Xu, L.D. Zhu, Mechanism study of the ethanol oxidation reaction on palladium in alkaline media, Electrochimica Acta 54 (8) (2009) 2203–2208, https://doi.org/10.1016/j.electacta.2008.10.034.
[55] Y.C. Weng, Y.G. Lee, Y.L. Hsiao, C.Y. Lin, A highly sensitive ascorbic acid sensor using a Ni-Pt electrode, Electrochim. Acta 56 (2011) 9937–9945, https://doi.org/10.1016/j.electacta.2011.08.084.
[56] X.W. Xie, J.J. Lv, L. Liu, A.J. Wang, J.J. Feng, Q.Q. Xu, Amino acid-assisted fabrication of uniform dendrite-like PtAu porous nanoclusters as highly efficient electrocatalyst for methanol oxidation and oxygen reduction reactions, Int. J. Hydrogen Energy 42 (2017) 2104–2115, https://doi.org/10.1016/j.ijhydene.2016.11.055.
[57] L.-L. Wang, D.-F. Zhang, L. Guo, Phase-segregated Pt–Ni chain-like nanohybrids with high electrocatalytic activity towards methanol oxidation reaction, Nanoscale 6 (2014) 4635, https://doi.org/10.1039/c4nr00139g.
[58] S. Mohanapriya, S. Suganthi, V. Raj, Mesoporous Pt–Ni catalyst and their electro catalytic activity towards methanol oxidation, J. Porous Mater. 24 (2017) 355–365, https://doi.org/10.1007/s10934-016-0268-y.
[59] E.S. Steigerwalt, G.A. Deluga, D.E. Cliffel, C.M. Lukehart, A Pt-Ru/graphitic carbon nanofiber nanocomposite exhibiting high relative performance as a direct-methanol fuel cell anode catalyst, J. Phys. Chem. B 105 (2001) 8097–8101, https://doi.org/10.1021/jp011633i.
[60] L. Zhang, X.F. Zhang, X.L. Chen, A.J. Wang, D.M. Han, Z.G. Wang, et al., Facile solvothermal synthesis of Pt71Co29 lamellar nanoflowers as an efficient catalyst for oxygen reduction and methanol oxidation reactions, J. Colloid Interface Sci. 536 (2019) 556–562, https://doi.org/10.1016/j.jcis.2018.10.080.
[61] R. Krishna, D.M. Fernandes, J. Ventura, C. Freire, E. Titus, Facile synthesis of reduced graphene oxide supported Pd@NixB/RGO nanocomposite: novel electrocatalyst for ethanol oxidation in alkaline media, Int. J. Hydrogen Energy 41 (2016) 11811–11822, https://doi.org/10.1016/j.ijhydene.2015.12.034.
[62] F. Ren, C. Zhai, M. Zhu, C. Wang, H. Wang, D. Bin, et al., Facile synthesis of PtAu nanoparticles supported on polydopamine reduced and modified graphene oxide as a highly active catalyst for methanol oxidation, Electrochim. Acta 153 (2015) 175–183, https://doi.org/10.1016/j.electacta.2014.11.184.
[63] K.W. Park, J.H. Choi, B.K. Kwon, S.A. Lee, Y.E. Sung, H.Y. Ha, et al., Chemical and electronic effects of Ni in Pt/Ni and Pt/Ru/Ni alloy nanoparticles in methanol electrooxidation, J. Phys. Chem. B 106 (2002) 1869–1877, https://doi.org/10.1021/jp013168v.
[64] J.W. Zhang, B. Zhang, X. Zhang, Enhanced catalytic activity of ternary NiCoPd nanocatalyst dispersed on carbon nanotubes toward methanol oxidation reaction in alkaline media, J. Solid State Electrochem. 21 (2017) 447–453, https://doi.org/10.1007/s10008-016-3331-3.
[65] Q. Jiang, L. Jiang, S. Wang, J. Qi, G. Sun, A highly active PtNi/C electrocatalyst for methanol electro-oxidation in alkaline media, Catal. Commun. 12 (2010) 67–70, https://doi.org/10.1016/j.catcom.2010.08.001.
[66] S. Ali, I. Khan, S.A. Khan, M. Sohail, R. Ahmed, Rehman A. ur, et al., Electrocatalytic performance of Ni@Pt core–shell nanoparticles supported on carbon nanotubes for methanol oxidation reaction, J. Electroanal. Chem. 795 (2017) 17–25, https://doi.org/10.1016/j.jelechem.2017.04.040.
[68] R.N. Singh, A. Singh, Anindita. Electrocatalytic activity of binary and ternary composite films of Pd, MWCNT and Ni, Part II: methanol electrooxidation in 1 M KOH, Int. J. Hydrogen Energy 34 (2009) 2052–2057, https://doi.org/10.1016/j.ijhydene.2008.12.047.
[69] I.M.A. Mohamed, K.A. Khalil, H.M. Mousa, N.A.M. Barakat, Ni/Pd-Decorated carbon NFs as an efficient electrocatalyst for methanol oxidation in alkaline medium, J. Electron. Mater. 46 (2017) 265–273, https://doi.org/10.1007/s11664-016-4900-z.
[70] A.E. Fetohi, R.S. Amin, R.M.A. Hameed, K.M. El-Khatib, Effect of nickel loading in Ni@Pt/C electrocatalysts on their activity for ethanol oxidation in alkaline medium,

Electrochim. Acta 242 (2017) 187–201, https://doi.org/10.1016/j.electacta.2017.05.022.
[71] W. Niu, L. Li, X. Liu, W. Zhou, W. Li, J. Lu, et al., One-pot synthesis of graphene/carbon nanospheres/graphene sandwich supported Pt3Ni nanoparticles with enhanced electrocatalytic activity in methanol oxidation, Int. J. Hydrogen Energy 40 (2014) 5106–5114, https://doi.org/10.1016/j.ijhydene.2015.02.095.
[72] L. Li, Y. Wu, J. Lu, C. Nan, Y. Li, Synthesis of Pt-Ni/graphene via in situ reduction and its enhanced catalyst activity for methanol oxidation, Chem. Commun. 49 (2013) 7486–7488, https://doi.org/10.1039/c3cc44514c.
[73] M.K. Jeon, K.R. Lee, H. Daimon, A. Nakahara, S.I. Woo, Pt45Ru45M10/C (M = Fe, Co, and Ni) catalysts for methanol electro-oxidation, Catal. Today 132 (2008) 123–126, https://doi.org/10.1016/j.cattod.2007.12.011.
[74] W. Huang, H. Wang, J. Zhou, J. Wang, P.N. Duchesne, D. Muir, et al., Highly active and durable methanol oxidation electrocatalyst based on the synergy of platinum–nickel hydroxide–graphene, Nat. Commun. 6 (2015) 10035, https://doi.org/10.1038/ncomms10035.
[75] S.H. Liu, W.Y. Yu, C.H. Chen, A.Y. Lo, B.J. Hwang, S.H. Chien, et al., Fabrication and characterization of well-dispersed and highly stable PtRu nanoparticles on carbon mesoporous material for applications in direct methanol fuel cell, Chem. Mater. 20 (2008) 1622–1628, https://doi.org/10.1021/cm702777j.
[76] J.-J. Lv, J.-N. Zheng, S.-S. Li, L.-L. Chen, A.-J. Wang, J.-J. Feng, Facile synthesis of Pt–Pd nanodendrites and their superior electrocatalytic activity, J. Mater. Chem. 2 (2014) 4384–4390, https://doi.org/10.1039/C3TA14304J.
[77] W. Huang, H. Wang, J. Zhou, J. Wang, P.N. Duchesne, D. Muir, et al., Highly active and durable methanol oxidation electrocatalyst based on the synergy of platinum-nickel hydroxide-graphene, Nat. Commun. 6 (2015) 10035, https://doi.org/10.1038/ncomms10035.